Journal of Alloys and Compounds 941 (2023) 169011

Contents lists available at ScienceDirect

Journal of Alloys and Compounds

journal homepage: www.elsevier.com/locate/jalcom

Research Article

Gas sensing properties of graphene oxide loaded with $SrTiO_3$ nanoparticles

Khaoula Kacem [a,b], Juan Casanova-Chafer [c], Sami Ameur [b,d], Mohamed Faouzi Nsib [a,b], Eduard Llobet [c,*]

[a] Higher School of Sciences and Technology of Hammam Sousse, University of Sousse, 4011, Tunisia
[b] NANOMISENE Laboratory, LR16CRMN01, Centre for Research on Microelectronics and Nanotechnology (CRMN), Technopole of Sousse, B.P334, 4054, Tunisia
[c] Universitat Rovira i Virgili, MINOS, Avda. Països Catalans, 26, 43007, Tarragona, Spain
[d] High Agronomic Institute of Chott Meriem, University of Sousse, 4042, Tunisia

ARTICLE INFO

Article history:
Received 12 September 2022
Received in revised form 15 December 2022
Accepted 21 January 2023
Available online 24 January 2023

Keywords:
Graphene oxide
$SrTiO_3$ perovskite
Gas sensor
NO_2
CO_2
NH_3

ABSTRACT

This paper reports a straightforward and inexpensive method for the fabrication of gas sensing devices based on graphene oxide (GO) synthesized by a modified Hummer's method and decorated with strontium titanate perovskite ($SrTiO_3$). The active layers developed were employed for the detection of hazardous gases such as NO_2, CO_2, and NH_3. The physical and chemical properties were also analyzed using various experimental techniques including field emission scanning electron microscopy (FESEM), transmission electron microscopy (TEM), X-ray powder diffraction (XRD), and Raman spectroscopy. Repeated response and recovery cycles were applied in the detection of nitrogen dioxide (NO_2), carbon dioxide (CO_2), and ammonia (NH_3). Accordingly, the gas sensing study reveals that decorated GO exhibits a high response towards NO_2 at an operating temperature of 100 °C with good sensitivity (up to 4-fold higher than that of pristine GO) and highly improved selectivity. Additionally, the effect of ambient humidity was tested for NO_2, demonstrating that GO/$SrTiO_3$ sensors show a good immunity to humidity cross-sensitivity. Lastly, a gas sensing mechanism was schematically proposed and discussed. These findings prove that the functionalization of GO with $SrTiO_3$ can overcome the limitations of GO-based sensors by enhancing their adsorption capability of gas molecules and their sensitivity towards target gases.

1. Introduction

Over the past few years, atmospheric pollutants emitted into the environment increased day by day as a result of industrial advancement and development, causing various human illnesses such as cancer, respiratory and cardiovascular diseases, central nervous system disorders, and many infectious diseases [1]. Not limited to this, air pollution contributes to global climate change and affects the entire planet [2]. Among toxic pollutants, gaseous species such as nitrogen dioxide, carbon monoxide, ammonia, and carbon dioxide represent a high challenge nowadays, because of their high toxicity and associated risk to the ecosystem, even in tiny quantities [3]. Hence, gas sensing and monitoring are essential for controlling industrial waste, environmental protection, and human safety [4].

Nowadays, the main interest of researchers is the development of high-quality gas sensors for the detection of various environmental hazardous pollutants. One of the most crucial characteristics of gas sensing materials is their large active surface area, which favors the adsorption of gas molecules, generally resulting in a better sensing performance [5]. Recently, graphene has attracted a great deal of interest in the field of gas sensors, owing to its two-dimensional structure which provides an extremely large surface area and a high carrier mobility [6]. However, the lack of oxygen functional groups in graphene structure limits its use in gas sensing applications, especially in its pristine form [7]. Nevertheless, graphene oxide (GO) contains abundant oxygen functional groups, such as hydroxyl, carboxyl, and epoxy groups, which can act as active sites and help increase the interaction with gas molecules [8–11]. Moreover, GO presents the advantage of its simple fabrication at a large scale with a good water solubility. However, the high density of oxygen functional groups usually reduces the conductivity of GO, which tends to behave as an electrical insulator.

Thus, several studies have reported the promising functionalization of graphene oxide to improve its sensing performance such as selectivity, sensitivity, stability, and operating temperature [12–14]. For instance, Kumar et al. studied the sensing properties of GO and

* Corresponding author.
E-mail address: eduard.llobet@urv.cat (E. Llobet).

https://doi.org/10.1016/j.jallcom.2023.169011

Para chloro benzoic acid (PCBA) functionalized GO, revealing an improved detection of ammonia when employing the functionalized GO [15]. Park et al. fabricated a gas sensor based on fluorinated GO and proved that fluorination also enhanced the ammonia gas sensing ability of GO-based gas sensors by lowering the Fermi level of GO and increasing the number of holes in GO [16]. Kumar et al. demonstrated that Meta Toluic acid functionalized graphene oxide has a potential application in ammonia gas sensing due to the formation of ester reactions, defects and carbon vacancies at the sensor surface, which enhances the interaction with NH_3 vapor molecules [17]. Jiang et al. developed sulfonic acid functionalized graphene oxide with high thermal stability and proved that the developed sensor provides a promising application as an electrochemical gas sensor to measure ethanol in the environment [18].

On the other hand, perovskite oxides (ABO_3) have attracted extensive attention in various areas owing to their exceptional properties [19]. Particularly, strontium titanate ($SrTiO_3$) is an n-type semiconductor that exhibits good thermal and chemical stability, with a 3.2 eV band gap, high dielectric constant, superconductivity, large absorption coefficient, and provides a large number of active sites. These properties make strontium titanate a promising material for gas sensing applications [20–22]. Previous works have reported the use of perovskite oxides in gas sensing applications. For example, Haron et al. demonstrated that lanthanum aluminate ($LaAlO_3$) exhibits high response and excellent selectivity towards ethanol [23]. Also, Zhang et al. showed that lanthanum ferrite ($LaFeO_3$) offered good gas sensing performance towards NO_2 [24]. Sun et al. reported the use of a rGO/$ZnSnO_3$ for the detection of formaldehyde (CH_2O) and showed that the developed sensor exhibited high sensing performance [25]. For instance, most of the published works related to the detection of toxic gases used bare perovskites, metal oxides, and graphene decorated with metal oxides. To the best of our knowledge, no report is available on graphene oxide decorated with strontium titanate perovskite.

In this work, we report the fabrication of a novel $SrTiO_3$ decorated graphene oxide chemoresistive gas sensor. Thus, pristine and functionalized graphene oxides were deposited on alumina substrates using an airbrush, which is a straightforward and inexpensive method. The sensing materials were characterized using several techniques such as field emission scanning electron microscopy (FESEM), transmission electron microscopy (TEM), Raman spectroscopy, and X-Ray diffraction (XRD). Sensors were tested for the detection of NO_2, CO_2, and NH_3 with different concentrations at an operating temperature of 100 ºC. It is anticipated that the decoration of GO with $SrTiO_3$ enhances the gas sensing performance of GO in terms of sensitivity, reproducibility, and stability.

2. Experimental section

2.1. Materials

Graphite (fine powder extra pure), Sodium nitrate (ACS reagent, ≥99.0 %), Sulfuric acid (99.999 %), Potassium permanganate (ACS reagent, ≥99.0 %), Hydrogen peroxide (30 %), Ethanol (absolute), and Strontium titanate (powder, 99 %) were purchased from Sigma Aldrich and used without further purification.

2.2. Synthesis of GO/$SrTiO_3$ nanocomposite

GO was synthesized from natural graphite powder through modified Hummer's method following a reported work [26]. Thus, 2 g of graphite and 1.25 g of sodium nitrate ($NaNO_3$) were added to 23 ml of concentrated sulphuric acid (H_2SO_4) under magnetic stirring for 20 min in an ice-water bath. Then, about 7.5 g of potassium permanganate ($KMnO_4$) were carefully added and stirring was continued for 2 h. Subsequently, the mixture was removed from the ice bath and stirred again at T = 30 °C for 30 min. After that, 120 ml of distilled water were slowly added and the temperature of the reaction mixture was suddenly increased, obtaining a brown suspension. After 15 min of stirring at 90 °C, 350 ml of distilled water was added to the mixture and the heating was turned off. The suspension was further treated by adding hydrogen peroxide H_2O_2 (30 %) until the color of the solution became green. The solution was filtered and washed with distilled water to remove hydroxide ions (OH^-) and then dried overnight. The obtained powder was dispersed in an appropriate amount of distilled water and maintained in an ultrasonic bath for 1 h. Finally, after filtration and drying, a powder of exfoliated graphene oxide was obtained.

Afterwards, $SrTiO_3$ nanoparticles were decorated onto GO layers by simple chemical impregnation technique through vigorous stirring. Thus, 1 mg of the synthesized GO was added to 5 ml of ethanol and maintained in an ultrasonic bath until dispersion. In another glass vial, 1 mg of $SrTiO_3$ was dispersed in 5 ml of ethanol through sonication. Then, 1 ml of $SrTiO_3$ (20 %) was added to the GO suspension and stirred for 1 h. Finally, we obtained a mixture of GO/$SrTiO_3$. An additional bare GO suspension was prepared to act as a reference sample to study the effect of loading with $SrTiO_3$.

2.3. Fabrication of GO/$SrTiO_3$ sensor and gas sensing measurements

The obtained GO/$SrTiO_3$ mixture was deposited onto alumina substrates by the airbrush spraying technique, employing nitrogen as a carrier gas. The hot plate that supported alumina substrates was kept at 110 °C during the deposition process. The nanomaterials were deposited on platinum screen-printed electrodes as shown in Fig. 1. A similar procedure was followed for the fabrication of a bare GO sensor using the GO suspension. The electrical resistance of films can be monitored while coating the electrode area. Ensuring that baseline resistance is equal among different sensing devices using the same gas sensitive nanomaterial, has been shown to improve device-to-device reproducibility.

After that, the prepared sensors were placed in an airtight Teflon test chamber with a volume of 35 cm^3. The sensors were stabilized under synthetic dry air for 15 min before being exposed for 5 min to the desired gas diluted in synthetic air. The dilution rate was varied to expose sensors to several gas concentrations. Changes in sensor resistance were measured using an Agilent HP 34972 A multimeter while varying gas concentrations. The total flow was adjusted at a low rate of 100 ml/min to minimize the system's power consumption and allow it to operate under more realistic test conditions. The sensor response was calculated as the ratio $\Delta R/R_0$ (%) = $[(R-R_0)/R_0] \times 100$, where R_0 is the resistance of the sensor under dry air, and R is the resistance of the sensor under the target gas.

2.4. Material characterization

The physical and chemical characteristics of the bare and functionalized graphene oxide sensors were investigated by several techniques such as FESEM, TEM, XRD, and Raman spectroscopy. The surface morphology of the sensors was analyzed using field emission scanning electron microscopy (FESEM, Carl Zeiss AG - ULTRA 55). Moreover, transmission electron microscopy (TEM, JEOL JEM 2100 F) was used to investigate the morphology of the developed materials. Thus, bare GO and GO/$SrTiO_3$ were ultrasonically dispersed in ethanol. Then, a drop of each suspension was deposited on a holey carbon film supported by a 300-mesh copper grid. The crystallinity of the as-developed samples was determined by Raman spectroscopy (Renishaw plc) coupled to a confocal Leica DM2500 microscope (Leica Microsystems GmbH) using a green laser at the wavelength of 514 nm. Finally, the crystal structure of the obtained nanomaterials was investigated using X-ray diffraction (XRD, Philips X'Pert) equipped with a copper source (Cu-Ka radiation,

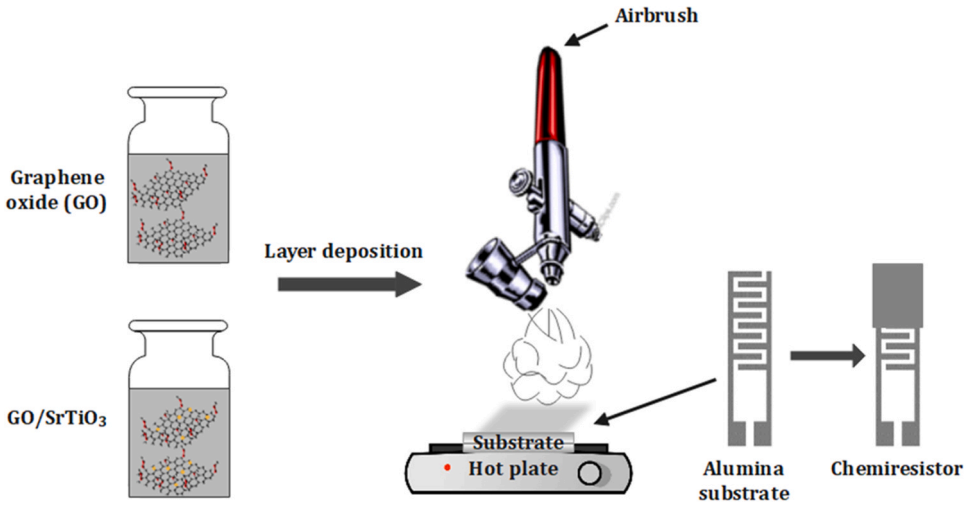

Fig. 1. Scheme of the sensor fabrication by airbrush.

λ = 0.154187 Å) in the 2θ range of 5–80. The nanomaterials were ultrasonically dispersed in ethanol and a drop of each dispersion was deposited onto a silicon wafer with (510) orientation.

3. Results and discussion

3.1. Morphological analysis

The morphological structure of the prepared GO and GO/$SrTiO_3$ sensors was studied using FESEM and transmission electron microscopy (TEM). Fig. 2a shows the morphology of graphene oxide sheets, which appear as wrinkled and folded layers. Fig. 2b shows the surface morphology of GO/$SrTiO_3$, clearly illustrating the stacking of $SrTiO_3$ particles onto GO layers, leading to a transformation in the surface morphology of GO in which the layers become segregated. Thereby, this result proves the successful formation of the GO/$SrTiO_3$ hybrid.

Fig. 3 depicts TEM images of both sensor types. The wrinkled folded layer structure of GO is confirmed in Fig. 3a, while the $SrTiO_3$ nanoparticles appear partially agglomerated in Fig. 3b, with an average diameter of 44 ± 1.66 nm. In addition, $SrTiO_3$ particles can be seen well embedded within GO sheets, indicative of the successful combination of SrTiO3 nanoparticles with GO to produce the GO/$SrTiO_3$ nanomaterial.

3.2. Raman spectroscopy

Raman spectroscopy was employed to study the structural defects of the as-prepared materials. Fig. 4 shows the Raman spectra for bare and functionalized graphene oxide. The spectrum of GO shows two obvious peaks: the D band at 1355 cm^{-1} originates from the density of defects in the material due to functionalization, doping, and the formation of sp^3 C-C atoms, and the G band at 1596 cm^{-1} corresponds to the E_{2g} symmetric stretching of the sp^2 hybridized C═C bond [27]. The spectrum of GO/$SrTiO_3$ revealed a variation in the D and G bands positions, which were shifted to 1351 cm^{-1} and 1599 cm^{-1}, respectively. In addition, the intensity ratio I_D/I_G was almost the same for GO (0.91) and GO/$SrTiO_3$ (0.89). Nevertheless, compared to the Raman spectrum of GO, the graphene's Raman peaks intensities were increased for decorated GO samples, which is probably due to the localized surface plasmon resonance (LSPR) effect of $SrTiO_3$ NPs induced by the laser (532 nm) [28]. It is worth mentioning that the increase in Raman intensities has been already shown in previous studies with graphene decorated with metal nanoparticles [29,30].

3.3. XRD analysis

Fig. 5 shows the X-ray diffraction results of the as-prepared materials. The diffraction pattern of GO reveals a sharp peak at 2θ = 11.75 corresponding to the (002) plane reflection. The XRD pattern of GO/$SrTiO_3$ shows peaks at 32.21°, 39.82°, 46.26°, 57.5°, and 67.58° related to the (110), (111), (200), (211), and (220) planes of the crystal structure of $SrTiO_3$, respectively, which match those of the standard card of $SrTiO_3$ (JCPDS Card No. 01-079-0176) [31]. Besides, the characteristic peak of GO was observed at 11.71º. This result confirms that GO was successfully decorated with $SrTiO_3$ [32].

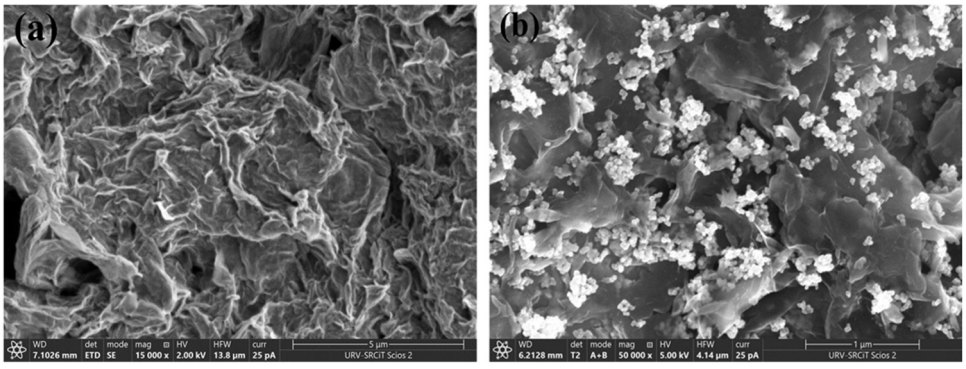

Fig. 2. FESEM images of GO (a) and GO/$SrTiO_3$ nanomaterials (b).

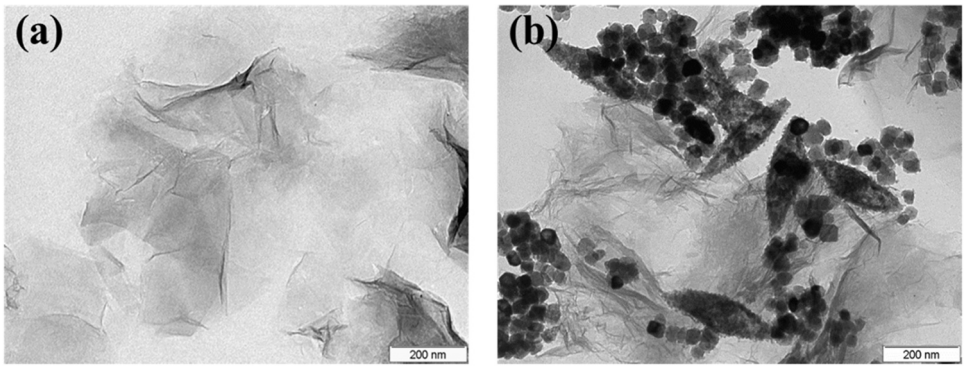

Fig. 3. TEM images of GO (a) and GO/$SrTiO_3$ nanomaterials (b).

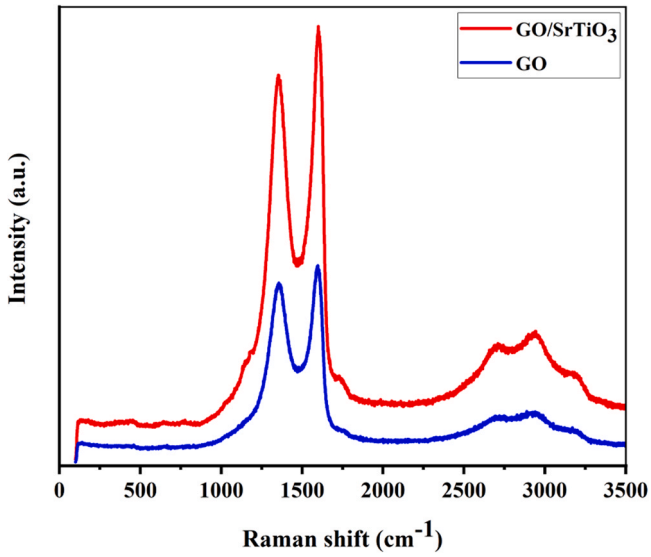

Fig. 4. Raman spectroscopy of GO and GO/$SrTiO_3$ samples.

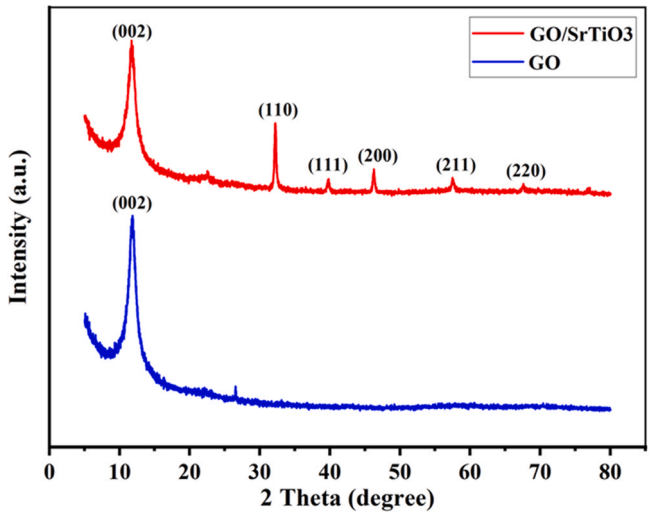

Fig. 5. XRD analysis of GO and GO/$SrTiO_3$.

3.4. Interaction between GO and $SrTiO_3$

The GO/$SrTiO_3$ hybrid is formed via an impregnation method. It is well-known that graphene, GO and reduced-GO films often behave as mild p-type semiconductors [4–7]. On the other hand, $SrTiO_3$ is an n-type semiconductor [20]. The existence of an interaction between the GO and the embedded $SrTiO_3$ nanoparticles in the hybrid film is proved by the strong difference existing between the baseline resistance of GO films and the one of GO/$SrTiO_3$ films. Typically, the baseline resistance in air of the GO/$SrTiO_3$ films studied here was 15-fold higher than the one of GO films. This difference can be explained by the fact that, once supported on GO, $SrTiO_3$ nanoparticles (n-type) inject electrons to the p-type GO. This electronic charge recombines with holes (i.e. the majority free charge carriers in GO), which results in an increased resistance of the GO/$SrTiO_3$ hybrid films.

4. Gas sensing results

The gas sensing properties of bare GO and $SrTiO_3$ functionalized GO were investigated by exposing the materials to nitrogen dioxide, carbon dioxide and ammonia, which are considered to be among the most abundant atmospheric pollutants. All measurements were conducted at an operating temperature of 100 ºC and the sensors were first stabilized under dry air for 15 min, followed by a 5-minute exposure to different concentrations of the target gases.

4.1. Nitrogen dioxide

Fig. 6a depicts the response plots of the sensors as a function of time while applying different concentrations of NO_2 (200, 400, 600, 800, and 1000 ppb). As it can be seen, both sensors present resistance decreases upon exposure to NO_2 (i.e., a reducing gas), which proves the p-type semiconducting characteristics of the materials. On the other hand, Fig. 6b reveals the calibration curves for the two types of sensors. As shown, there is a significant improvement in the response (up to 4-fold) when $SrTiO_3$ is decorating the GO. The enhanced sensing performance of the GO/$SrTiO_3$ sensor may be due to a higher reactivity of the perovskite oxide and higher surface area. Considering that sensitivity is defined as the slope of the calibration curve, then, it can be deduced that not only the response rate increases for the decorated graphene oxide but GO/$SrTiO_3$ shows also a higher sensitivity (up to 4-fold compared to the one of pristine GO). The repeatability of measurements was investigated by performing 5 replicated measurement cycles of increasing gas concentrations. Panel a) in Fig. 6 shows 3 of such cycles. Despite the changes in the baseline values (due to sensors being subject to strong gas concentration changes in relatively short time periods), the relative change in resistance (i.e., sensor response) is clearly repeatable over the different measurement cycles. The uncertainty associated to measurements is indicated by the error bars added to the calibration curves sown in panel b) of Fig. 6. This uncertainty remains below 17 %, which is fair considering again that sensors are exposed to strong gas concentration variations in a limited period of time. Besides, to investigate their selectivity, both sensors were tested for the detection of different reducing and oxidizing toxic gases.

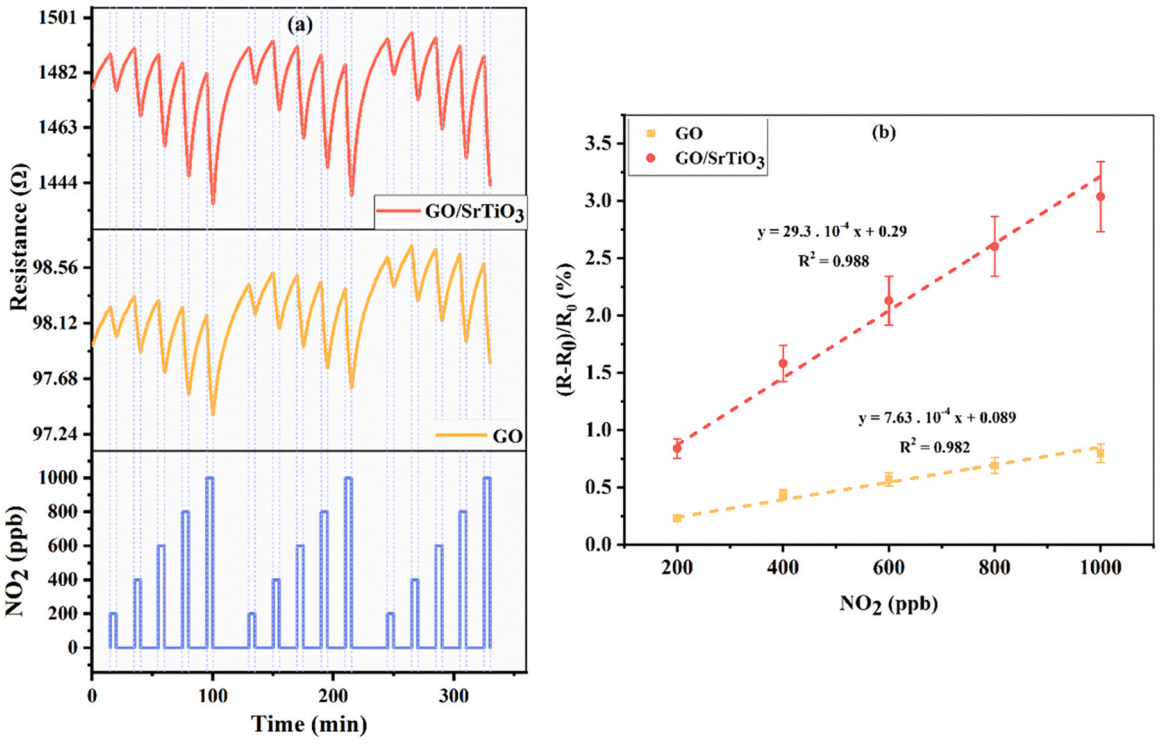

Fig. 6. Variation of sensors resistance as a function of time with increasing NO_2 concentration at an operating temperature of 100 ºC (a) and calibration curves for bare and decorated graphene oxide (b).

4.2. Carbon dioxide

The developed sensors were also tested for detecting carbon dioxide. Hence, repeated response and recovery cycles to different concentrations (20, 40, 60, 80, and 100 ppm) were performed at 100 ºC (Fig. 7a). As expected, the resistance of both sensors increases while exposed to CO_2, which acts as a reducing gas (electron donor) [33]. Fig. 7b shows the calibration curves for the two types of sensors, as well as their sensitivity. As it can be observed, a higher sensitivity towards CO_2 was obtained for graphene oxide decorated with $SrTiO_3$, compared to bare graphene oxide. Despite the changes in the baseline values, the relative change in resistance (i.e., sensor

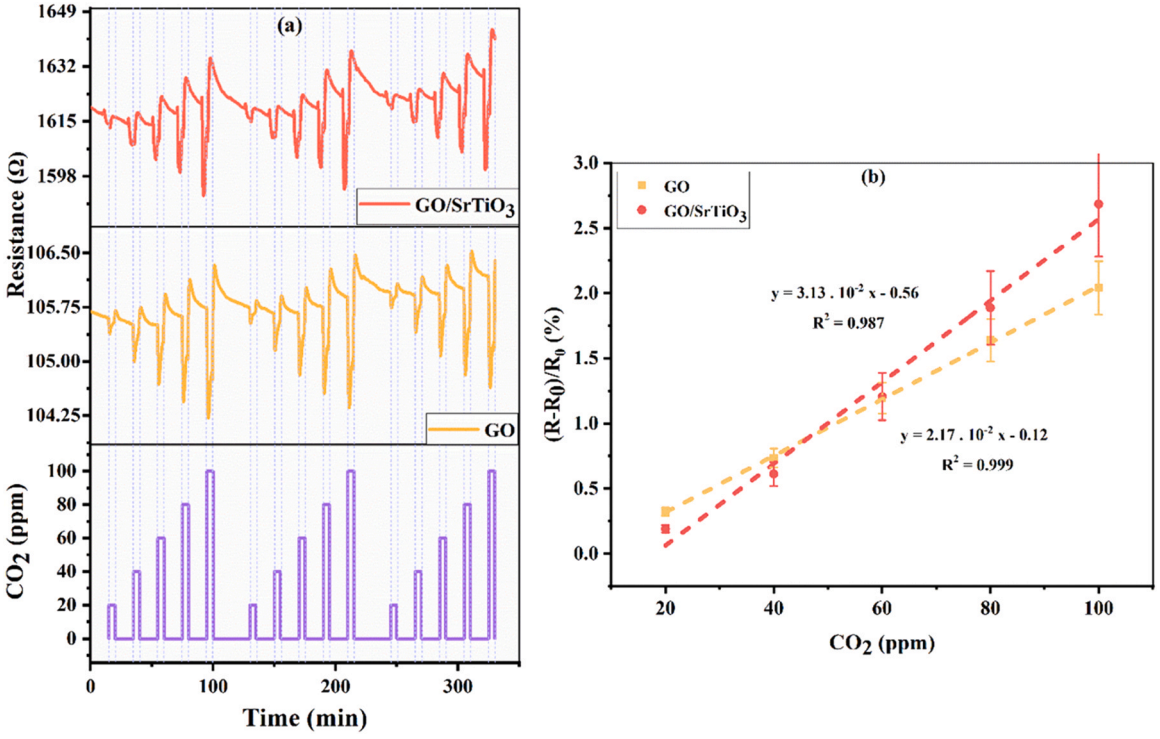

Fig. 7. Variation of sensors resistance in the function of time with increasing CO_2 concentration at 100 ºC (a) and calibration curves for bare and decorated graphene oxide (b).

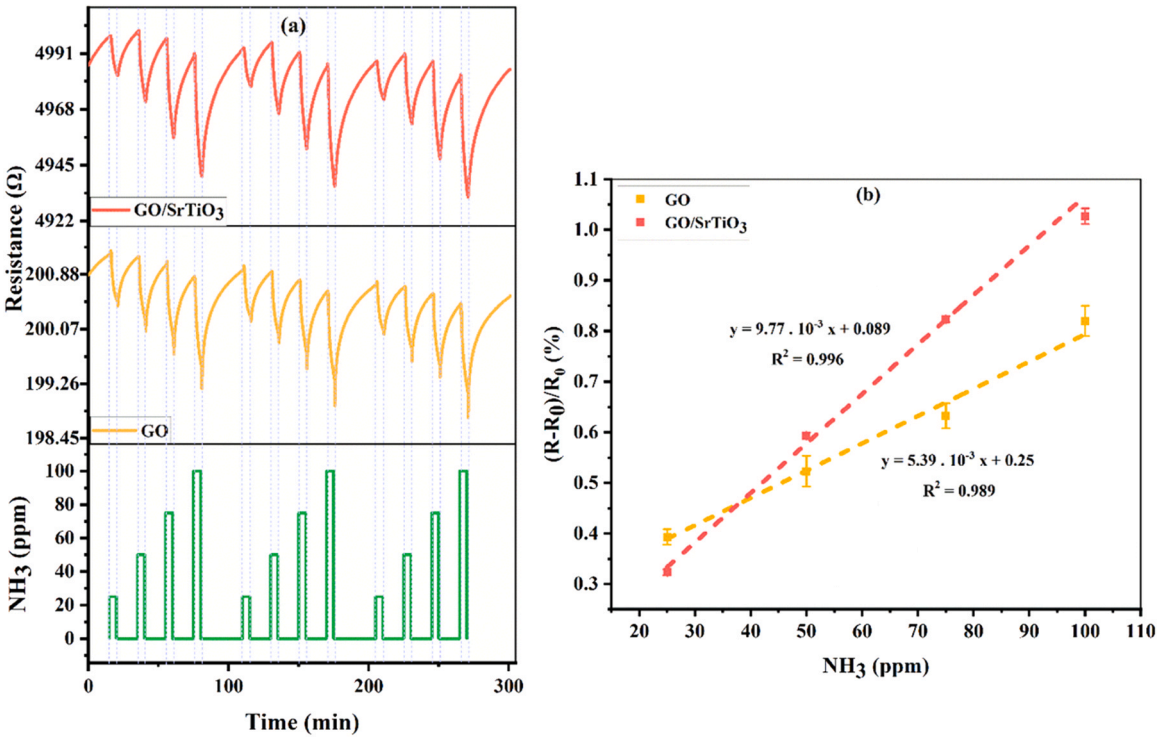

Fig. 8. Variation of sensor resistance as a function of time with increasing NH_3 concentrations at an operating temperature of 100 ºC (a) and calibration curves for bare and decorated graphene oxide (b).

response) is fairly repeatable over the different measurement cycles. The uncertainty associated to measurements is indicated by the error bars added to the calibration curves sown in panel b) of Fig. 7. Uncertainty averages 30 % and clearly worsens in respect to the one previously found for NO_2. This is due to the presence of initial overshots in the response to CO_2.

4.3. Ammonia

NH_3 detection was analyzed by exposing the sensors to repeated response and recovery cycles of four ammonia concentrations (25, 50, 75, and 100 ppm) at 100 ºC. Both sensors show a decrease in their resistance while exposed to NH_3 (Fig. 8a), proving that NH_3 was acting as electron withdrawing under the applied experimental conditions. In a similar way to what was found during the measurements of nitrogen dioxide and carbon dioxide, graphene oxide decorated with $SrTiO_3$ showed a higher response and sensitivity (up to 2-fold) towards ammonia than bare graphene oxide did (Fig. 8b). Again, despite the changes in the baseline values, the relative change in resistance (i.e., sensor response) is highly repeatable over the different measurement cycles. The uncertainty associated to measurements is indicated by the error bars added to the calibration curves sown in panel b) of Fig. 8. Uncertainty remains below 10 %.

Results are summarized in Table 1, which shows the sensitivities of the two types of sensors. Graphene oxide decorated with $SrTiO_3$ presents a better sensitivity for all the gases studied compared to pristine GO, and the best performance was observed for nitrogen dioxide. This result confirms that the developed sensors are highly sensitive to nitrogen dioxide and agrees with previous DFT calculations [34,35]. This higher response for nitrogen dioxide may be due to the charge transfer between graphene and the nitrogen oxide molecule (+0.77), which is significantly higher than for NH_3 (−0.10) and CO_2 (+0.01).

Table 1
Sensor sensitivity (10^{-2} × ppm^{-1}).

	GO	GO/$SrTiO_3$
NO_2	76.3	293
CO_2	2.17	3.13
NH_3	0.539	0.977

Furthermore, the limit of detection (LOD) towards NO_2 was estimated according to the following equation:

LOD = 3 (Sy/b) where Sy is the standard deviation of y-residuals and b corresponds to the slope of the calibration curve (sensitivity)·Hence, the GO has a LOD of 158 ppb, whereas the decorated GO reveals a LOD of 72 ppb·

Besides the stability of operation of the different nanomaterials used, demonstrated by the repeatability of results and the fair uncertainty associated to the gas measurements, the long term stability of sensor response was also investigated. The measurement process took three months to complete. Over this period, nitrogen dioxide, ammonia and carbon dioxide were measured repeated times and the response of sensors remained stable, within the uncertainty ranges discussed above. Additionally, carbon dioxide and ammonia were measured again three months after the measurement process was completed. During this 3-month elapsed period sensors were stored in air, without any particular conditions and the new responses were very similar to the previous ones (below 10 % decrease in response on average).

4.4. Selectivity analysis

Fig. 9 illustrates the selectivity analysis by comparing the responses towards NO_2, CO_2 and NH_3. Despite the concentration of nitrogen dioxide being at least 20 times lower than for carbon dioxide or ammonia, the response of GO/$SrTiO_3$ to NO_2 is one order of magnitude higher than for the other two species. Defining selectivity towards NO_2 as follows:

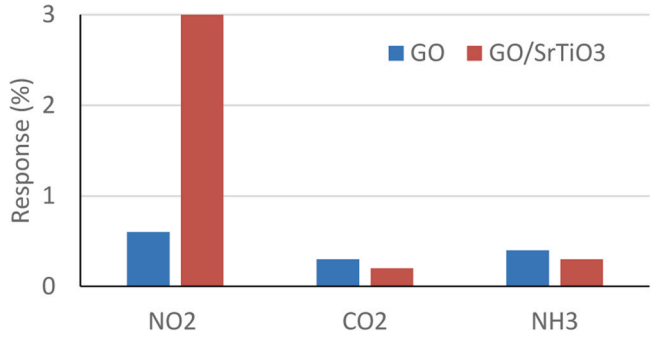

Fig. 9. Selectivity analysis. Comparison of the responses towards NO_2 (1 ppm), CO2 (20 ppm) and NH_3 (25 ppm) for GO and GO/$SrTiO_3$ sensors.

$$S_{NO2} = R_{NO2,\ 1\ ppm}/[\ R_{NO2,\ 1\ ppm} + R_{\ CO2,\ 20\ ppm} + R_{\ NH3,\ 25\ ppm}]$$

The closer to unity S_{NO2} is, the higher the selectivity towards NO_2 is. S_{NO2} is 0.86 for GO/$SrTiO_3$ and 0.46 for GO, which clearly indicates that GO/$SrTiO_3$ sensors are remarkably more selective than GO sensors. This superior selectivity is also supported by the significantly higher sensitivity of GO/$SrTiO_3$ towards NO_2 (see Table 1), compared to any other species tested.

Table 2 summarizes a comparison between the performance in the detection of NO_2 for the prepared GO/$SrTiO_3$ sensor device and the performance of other, previously reported, graphene hybrid sensors. Most of the previously reported results do not study the effect of humidity in sensor response, nor discuss long-term stability issues, nor estimate a limit of detection for NO_2. Additionally, the flow rates used during measurements are larger than the one used here, and this is known to enhance sensor response. Considering the operating temperature, the low concentrations detected and the high response achieved, the GO/$SrTiO_3$ sensors are among the best state-of-the-art sensors. Finally, taking also into account the high improvement achieved in selectivity via loading GO with $SrTiO_3$, it can be derived that an outstanding NO_2 sensing performance for the GO decorated with $SrTiO_3$ material has been achieved.

4.5. Humidity test

The humidity impact on gas sensing performance was studied for NO_2. Fig. 10 depicts a comparison of the sensing responses under dry and humid environments (60 % R.H. @25ºC), when employing the $SrTiO_3$ decorated GO. Under humid conditions, the response towards nitrogen dioxide remained stable and slightly decreased in comparison to dry conditions. Indeed, these similar responses are interesting from the gas sensing point of view, since ambient moisture is considered to be one of the main interfering species in chemoresistive devices.

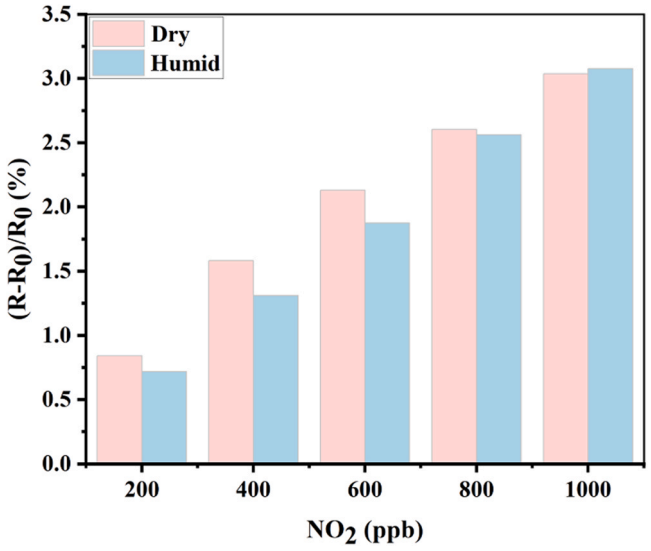

Fig. 10. Comparison of the sensing response towards NO_2 for GO decorated with $SrTiO_3$ under dry and humid (60 % R.H.) conditions at an operating temperature of 100 ºC.

4.6. Gas sensing mechanism

It is well known that GO presents a high density of oxygen functional groups such as hydroxyl, epoxy on its basal plane sheets and carboxyl groups on its edges [40]. This provides large active sites for adsorption of gas molecules, and thus facilitates the charge tranfer between GO and the target gas [41]. Hence, according to our gas sensing measurements, GO is responsive towards NO_2, CO_2, and NH_3. However, as expected from the literature, limited sensitivity was observed, probably originated from its poor conductivity derived from the oxidation process. Nevertheless, the presence of $SrTiO_3$ in GO layers was favorable for detecting the target gases, and higher responses and sensitivities were found for all the tested gases.

The improved gas sensing performance of graphene oxide decorated with $SrTiO_3$ can be probably attributed to the high reactivity of $SrTiO_3$ and the interaction existing between the perovskite and GO nanomaterial. The mechanism behind this enhancement is schematically presented in Fig. 11, and discussed to better understand the impact of $SrTiO_3$ on GO gas sensing properties.

Accordingly, the exposure to a target gas increases or decreases sensor resistance, depending on the type of the dominant carriers in the material and the gas species (oxidizing or reducing) [42]. Despite $SrTiO_3$ exhibits an n-type semiconductor behavior, the GO/$SrTiO_3$ nanocomposite acts similarly to a p-type semiconductor, owing to the weigth predominance of GO. Thus, when bare GO or GO/$SrTiO_3$ interact with an oxidizing gas (electron acceptor nature) such as NO_2, the sensors resistance decreases. On the other hand, the interaction with a reducing gas such as CO_2, leads to a higher sensor

Table 2
Comparison of NO_2 sensing performance for GO/$SrTiO_3$ and other previous works.

Material-based sensor	T (°C)	NO_2 (ppm)	Response (%)	T_{resp}/T_{rec} (sec)	Sensitivity (ppm^{-1})	LOD (ppb)	Ref.
GO/$SrTiO_3$	100	1	3.2	300/900	2.93	72	This work
MOS_2/Graphene	100	5	6.83	300/1800	N.A.	1200	[34]
rGO/Au NPs	150	50	3.2	135/136	N.A.	N.A.	[35]
3D SnO_2/rGO	55	100	7.3	> 310	N.A.	N.A.	[36]
WS_2/Graphene	180	2	3	600/600	N.A.	15	[37]
SnS_2/rGO	80	11.9	56.8	360/3180	N.A.	N.A.	[38]
Au/rGO	50	5	1.33	132/386	N.A.	N.A.	[39]

T_{resp}: Response time; T_{rec}: Recovery time.

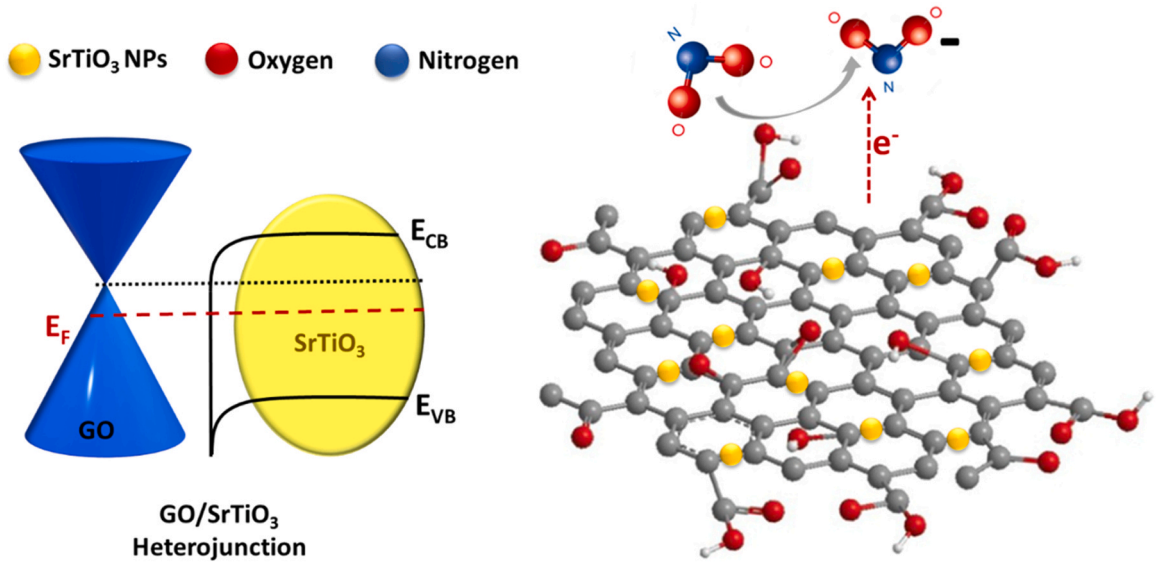

Fig. 11. Gas sensing mechanism of the GO/$SrTiO_3$ nanomaterial.

resistance. In the case of NO_2, the oxygen functional groups present in GO promote the adsorption of nitrogen dioxide molecules, creating more holes in the material, and thus decreasing sensor resistance. Moreover, the incorporation of $SrTiO_3$ perovskite in graphene oxide results in the injection of electrons from the n-type strontium titanate to the p-type GO, which increases the resistance of the loaded GO layer [43,44]. This explains the higher baseline resistance observed for GO/ $SrTiO_3$ sensors in comparison to the one of the pure GO sensor.

Overall, when atmospheric oxygen interacts with the active layers, it traps electrons from the conduction band (in our case from both, the GO and $SrTiO_3$), resulting in a depletion layer in which positive carriers (holes) are accumulated. Additionally, when sensors are exposed to NO_2, further electrons are trapped. The n-type $SrTiO_3$ nanoparticles supported by the GO layer offer an increased number of sites for adsorbing NO_2. Upon adsorption, electronic charge is transferred from the GO to $SrTiO_3$ nanoparticles, which results in a large resistance decrease. This electronic senzitization effect explains why GO/ $SrTiO_3$ nanomaterials show higher response to NO_2 than bare GO.

5. Conclusion

In this study, we have successfully fabricated a gas sensor device based on decorated graphene oxide (GO) with strontium titanate perovskite ($SrTiO_3$) for the detection of NO_2, CO_2 and NH_3. The GO/ $SrTiO_3$ sensing device was developed using a simple and inexpensive technique. FESEM, TEM, XRD and Raman spectroscopy clearly demonstrated the growth of $SrTiO_3$ NPs on graphene oxide sheets. Moreover, we have studied the gas sensing performance of both pristine and decorated GO. The sensing results showed that pristine GO gas sensors present generally weaker sensing properties than GO decorated with $SrTiO_3$. Particularly, GO/$SrTiO_3$ exhibits the highest response and sensitivity towards NO_2, when compared to NH_3 and CO_2. This can be due to the presence of $SrTiO_3$ nanoparticles, which facilitate further the adsorption of nitrogen dioxide, thus enhancing the charge transfer between the GO, $SrTiO_3$ and adsorbed NO_2 molecules. Not limited to this, GO/$SrTiO_3$ gas sensing devices exhibit a low limit of detection of 72 ppb for NO_2, which is much lower than that of pristine GO and a stable response towards NO_2, even under different humidity levels.

CRediT authorship contribution statement

Khaoula Kacem: Investigation, Formal analysis, Visualization, Writing – original draft. **Juan Casanova-Chafer:** Investigation, Data curation, Methodology, Resources, Writing – review & editing. **Sami Ameur:** Conceptualization, Writing – review & editing. **Mohamed Faouzi Nsib:** Conceptualization, Funding acquisition, Supervision, Writing – review & editing. **Eduard Llobet:** Conceptualization, Funding acquisition, Supervision, Writing – review & editing.

Data availability

Data will be made available on request.

Declaration of Competing Interest

The authors declare that they have no known competing financial interests or personal relationships that could have appeared to influence the work reported in this paper.

Acknowledgements

Khaoula Kacem would like to thank her father Adel Kacem for funding her visiting researcher in Rovira i Virgili University, MINOS group to finish this work. E.L. is supported by the Catalan Institution for Research and Advanced Studies via the 2018 Edition of the ICREA Academia Award.

References

[1] I. Manisalidis, E. Stavropoulou, A. Stavropoulos, E. Bezirtzoglou, Environmental and health impacts of air pollution: a review, Front. Public Health 8 (2020) 14, https://doi.org/10.3389/fpubh.2020.00014
[2] R. Sivarethinamohan, S. Sujatha, S. Priya, A. Sankaran, Z. Gafoor, Rahman, Impact of air pollution in health and socio-economic aspects: review on future approach, Mater. Today Proc. 37 (2021) 2725–2729, https://doi.org/10.1016/j.matpr.2020.08.540
[3] S. Gupta Chatterjee, S. Chatterjee, A.K. Ray, A.K. Chakraborty, Graphene–metal oxide nanohybrids for toxic gas sensor: a review, Sens. Actuators B Chem. 221 (2015) 1170–1181, https://doi.org/10.1016/j.snb.2015.07.070
[4] W. Tian, X. Liu, W. Yu, Research progress of gas sensor based on graphene and its derivatives: a review, Appl. Sci. 8 (2018) 1118, https://doi.org/10.3390/app8071118
[5] S. Varghese, S. Varghese, S. Swaminathan, K. Singh, V. Mittal, Two-dimensional materials for sensing: graphene and beyond, Electronics 4 (2015) 651–687, https://doi.org/10.3390/electronics4030651

[6] X. Tang, M. Debliquy, D. Lahem, Y. Yan, J.-P. Raskin, A review on functionalized graphene sensors for detection of ammonia, Sensors 21 (2021) 1443, https://doi.org/10.3390/s21041443

[7] S.M. Majhi, A. Mirzaei, H.W. Kim, S.S. Kim, Reduced graphene oxide (rGO)-loaded metal-oxide nanofiber gas sensors: an overview, Sensors 21 (2021) 1352, https://doi.org/10.3390/s21041352

[8] K. Toda, R. Furue, S. Hayami, Recent progress in applications of graphene oxide for gas sensing: a review, Anal. Chim. Acta 878 (2015) 43–53, https://doi.org/10.1016/j.aca.2015.02.002

[9] H. Rashidi Nodeh, H. Sereshti, Synthesis of magnetic graphene oxide doped with strontium titanium trioxide nanoparticles as a nanocomposite for the removal of antibiotics from aqueous media, RSC Adv. 6 (2016) 89953–89965, https://doi.org/10.1039/C6RA18341G

[10] Y.R. Choi, Y.-G. Yoon, K.S. Choi, J.H. Kang, Y.-S. Shim, Y.H. Kim, H.J. Chang, J.-H. Lee, C.R. Park, S.Y. Kim, H.W. Jang, Role of oxygen functional groups in graphene oxide for reversible room-temperature NO2 sensing, Carbon 91 (2015) 178–187, https://doi.org/10.1016/j.carbon.2015.04.082

[11] K.V.A. Kumar, B. Lakshminarayana, D. Suryakala, Ch Subrahmanyam, Reduced graphene oxide supported ZnO quantum dots for visible light-induced simultaneous removal of tetracycline and hexavalent chromium, RSC Adv. 10 (2020) 20494–20503, https://doi.org/10.1039/D0RA02062A

[12] G.J. Thangamani, K. Deshmukh, T. Kovářík, N.A. Nambiraj, D. Ponnamma, K.K. Sadasivuni, H.P.S.A. Khalil, S.K.K. Pasha, Graphene oxide nanocomposites based room temperature gas sensors: a review, Chemosphere 280 (2021) 130641, https://doi.org/10.1016/j.chemosphere.2021.130641

[13] S. Prezioso, F. Perrozzi, L. Giancaterini, C. Cantalini, E. Treossi, V. Palermo, M. Nardone, S. Santucci, L. Ottaviano, Graphene oxide as a practical solution to high sensitivity gas sensing, J. Phys. Chem. C 117 (2013) 10683–10690, https://doi.org/10.1021/jp3085759

[14] Z.D. Leve, E.I. Iwuoha, N. Ross, The synergistic properties and gas sensing performance of functionalized graphene-based sensors, Materials 15 (2022) 1326, https://doi.org/10.3390/ma15041326

[15] R. Kumar, R. Singh, A. Kumar, R. Kashyap, D. Kumar, M. Kumar, Chemically functionalized graphene oxide thin films for selective ammonia gas sensing, Mater. Res. Express 7 (2020) 015612, https://doi.org/10.1088/2053-1591/ab66f1

[16] M.-S. Park, K.H. Kim, M.-J. Kim, Y.-S. Lee, NH 3 gas sensing properties of a gas sensor based on fluorinated graphene oxide, Colloids Surf. A Physicochem. Eng. Asp. 490 (2016) 104–109, https://doi.org/10.1016/j.colsurfa.2015.11.028

[17] R. Kumar, A. Kumar, R. Singh, R. Kashyap, R. Kumar, D. Kumar, S.K. Sharma, M. Kumar, Room temperature ammonia gas sensor using Meta Toluic acid functionalized graphene oxide, Mater. Chem. Phys. 240 (2020) 121922, https://doi.org/10.1016/j.matchemphys.2019.121922

[18] G. Jiang, M. Goledzinowski, F.J.E. Comeau, H. Zarrin, G. Lui, J. Lenos, A. Veileux, G. Liu, J. Zhang, S. Hemmati, J. Qiao, Z. Chen, Free-standing functionalized graphene oxide solid electrolytes in electrochemical gas sensors, Adv. Funct. Mater. 26 (2016) 1729–1736, https://doi.org/10.1002/adfm.201504604

[19] J. Casanova-Cháfer, R. García-Aboal, P. Atienzar, E. Llobet, Gas sensing properties of perovskite decorated graphene at room temperature, Sensors 19 (2019) 4563, https://doi.org/10.3390/s19204563

[20] B. Szafraniak, Ł. Fuśnik, J. Xu, F. Gao, A. Brudnik, A. Rydosz, Semiconducting metal oxides: SrTiO3, BaTiO3 and BaSrTiO3 in gas-sensing applications: a review, Coatings 11 (2021) 185, https://doi.org/10.3390/coatings11020185

[21] D.D. Kajale, G.E. Patil, V.B. Gaikwad, S.D. Shinde, D.N. Chavan, N.K. Pawar, S.R. Shirsath, G.H. Jain, Synthesis of $SrTiO_3$ nanopowder by sol-gel-hydrothemal method for gas sensing application, Int. J. Smart Sens. Intell. Syst. 5 (2012) 382–400, https://doi.org/10.21307/ijssis-2017-487

[22] B.L. Phoon, C.W. Lai, J.C. Juan, P.-L. Show, W.-H. Chen, A review of synthesis and morphology of SrTiO3 for energy and other applications, Int. J. Energy Res. 43 (2019) 5151–5174, https://doi.org/10.1002/er.4505

[23] W. Haron, A. Wisitsoraat, S. Wongnawa, Nanostructured perovskite oxides – LaMO3 (M=Al, Co, Fe) prepared by co-precipitation method and their ethanol-sensing characteristics, Ceram. Int. 43 (2017) 5032–5040, https://doi.org/10.1016/j.ceramint.2017.01.013

[24] X.-D. Zhang, W.-L. Zhang, Z.-X. Cai, Y.-K. Li, Y. Yamauchi, X. Guo, LaFeO3 porous hollow micro-spindles for NO2 sensing, Ceram. Int. 45 (2019) 5240–5248, https://doi.org/10.1016/j.ceramint.2018.11.221

[25] J. Sun, S. Bai, Y. Tian, Y. Zhao, N. Han, R. Luo, D. Li, A. Chen, Hybridization of ZnSnO3 and rGO for improvement of formaldehyde sensing properties, Sens. Actuators B Chem. 257 (2018) 29–36, https://doi.org/10.1016/j.snb.2017.10.015

[26] K. Kacem, Bio-reduction of graphene oxide using pomegranate peels for NO2 sensing and photocatalysis applications, J Mater. Sci., (n.d.) 14.

[27] R. Paul, R.N. Gayen, S. Biswas, S.V. Bhat, R. Bhunia, Enhanced UV detection by transparent graphene oxide/ZnO composite thin films, RSC Adv. 6 (2016) 61661–61672, https://doi.org/10.1039/C6RA05039E

[28] S.A. Ghopry, M.A. Alamri, R. Goul, R. Sakidja, J.Z. Wu, Extraordinary sensitivity of surface-enhanced raman spectroscopy of molecules on MoS2 (WS2) nanodomes/graphene van der waals heterostructure substrates, Adv. Opt. Mater. 7 (2019) 1801249, https://doi.org/10.1002/adom.201801249

[29] X.-J. Chen, G. Cabello, D.-Y. Wu, Z.-Q. Tian, Surface-enhanced Raman spectroscopy toward application in plasmonic photocatalysis on metal nanostructures, J. Photochem. Photobiol. C Photochem. Rev. 21 (2014) 54–80, https://doi.org/10.1016/j.jphotochemrev.2014.10.003

[30] R. Lu, A. Konzelmann, F. Xu, Y. Gong, J. Liu, Q. Liu, M. Xin, R. Hui, J.Z. Wu, High sensitivity surface enhanced Raman spectroscopy of R6G on in situ fabricated Au nanoparticle/graphene plasmonic substrates, Carbon 86 (2015) 78–85, https://doi.org/10.1016/j.carbon.2015.01.028

[31] M. Akilarasan, E. Tamilalagan, S.-M. Chen, S. Maheshwaran, T.-W. Chen, A.M. Al-Mohaimeed, W.A. Al-Onazi, M.S. Elshikh, An eco-friendly low-temperature synthetic approach towards micro-pebble-structured GO@SrTiO3 nanocomposites for the detection of 2,4,6-trichlorophenol in environmental samples, Microchim. Acta 188 (2021) 72, https://doi.org/10.1007/s00604-021-04729-w

[32] P.K. Gopi, B. Muthukutty, S.-M. Chen, T.-W. Chen, X. Liu, A.A. Alothman, M.A. Ali, S.M. Wabaidur, Platelet-structured strontium titanate perovskite decorated on graphene oxide as a nanocatalyst for electrochemical determination of neurotransmitter dopamine, New J. Chem. 44 (2020) 18431–18441, https://doi.org/10.1039/D0NJ03564E

[33] S. Behi, J. Casanova-Chafer, E. González, N. Bohli, E. Llobet, A. Abdelghani, Metal loaded nano-carbon gas sensor array for pollutant detection, Nanotechnology 33 (2022) 195501, https://doi.org/10.1088/1361-6528/ac4e43

[34] B. Cho, J. Yoon, S.K. Lim, A.R. Kim, D.-H. Kim, S.-G. Park, J.-D. Kwon, Y.-J. Lee, K.-H. Lee, B.H. Lee, H.C. Ko, M.G. Hahm, Chemical sensing of 2D graphene/MoS_2 heterostructure device, ACS Appl. Mater. Interfaces 7 (2015) 16775–16780, https://doi.org/10.1021/acsami.5b04541

[35] S. Rattan, S. Kumar, J.K. Goswamy, Gold nanoparticle decorated graphene for efficient sensing of NO2 gas, Sens. Int. 3 (2022) 100147, https://doi.org/10.1016/j.sintl.2021.100147

[36] L. Li, S. He, M. Liu, C. Zhang, W. Chen, Three-dimensional mesoporous graphene aerogel-supported SnO_2 nanocrystals for high-performance NO_2 gas sensing at low temperature, Anal. Chem. 87 (2015) 1638–1645, https://doi.org/10.1021/ac503234e

[37] W. Yan, M.A. Worsley, T. Pham, A. Zettl, C. Carraro, R. Maboudian, Effects of ambient humidity and temperature on the NO2 sensing characteristics of WS2/graphene aerogel, Appl. Surf. Sci. 450 (2018) 372–379, https://doi.org/10.1016/j.apsusc.2018.04.185

[38] M. Shafiei, J. Bradford, H. Khan, C. Piloto, W. Wlodarski, Y. Li, N. Motta, Low-operating temperature NO2 gas sensors based on hybrid two-dimensional SnS2-reduced graphene oxide, Appl. Surf. Sci. 462 (2018) 330–336, https://doi.org/10.1016/j.apsusc.2018.08.115

[39] H. Zhang, Q. Li, J. Huang, Y. Du, S. Ruan, Reduced graphene Oxide/Au nanocomposite for NO2 sensing at low operating temperature, Sensors 16 (2016) 1152, https://doi.org/10.3390/s16071152

[40] A.T. Dideikin, A.Y. Vul', Graphene oxide and derivatives: the place in graphene family, Front. Phys. 6 (2019) 149, https://doi.org/10.3389/fphy.2018.00149

[41] F. Li, X. Jiang, J. Zhao, S. Zhang, Graphene oxide: a promising nanomaterial for energy and environmental applications, Nano Energy 16 (2015) 488–515, https://doi.org/10.1016/j.nanoen.2015.07.014

[42] P. Shankar, J.B.B. Rayappan, Gas sensing mechanism of metal oxides: the role of ambient atmosphere, type of semiconductor and gases - a review, Sci. Lett. 4 (2015) 19.

[43] T. Pisarkiewicz, W. Maziarz, A. Małolepszy, L. Stobiński, D.A. Michoń, A. Szkudlarek, M. Pisarek, J. Kanak, A. Rydosz, Nitrogen dioxide sensing using multilayer structure of reduced graphene oxide and α-Fe2O3, Sensors 21 (2021) 1011, https://doi.org/10.3390/s21031011

[44] N. Sharma, H.S. Kushwaha, S.K. Sharma, K. Sachdev, Fabrication of $LaFeO_3$ and rGO-$LaFeO_3$ microspheres based gas sensors for detection of NO_2 and CO, RSC Adv. 10 (2020) 1297–1308, https://doi.org/10.1039/C9RA09460A